

Global survey of star clusters in the Milky Way

III. 139 new open clusters at high Galactic latitudes

S. Schmeja¹, N. V. Kharchenko^{1,2}, A. E. Piskunov^{1,3}, S. Röser¹, E. Schilbach¹, D. Froebrich⁴, and R.-D. Scholz⁵

¹ Astronomisches Rechen-Institut, Zentrum für Astronomie der Universität Heidelberg, Mönchhofstr. 12-14, 69120 Heidelberg, Germany

e-mail: sschmeja@ari.uni-heidelberg.de

² Main Astronomical Observatory, 27 Academica Zabolotnogo Str., 03680 Kiev, Ukraine

³ Institute of Astronomy of the Russian Academy of Sciences, 48 Pyatnitskaya Str., 109017 Moscow, Russia

⁴ Centre for Astrophysics and Planetary Science, University of Kent, Canterbury, CT2 7NH, United Kingdom

⁵ Leibniz-Institut für Astrophysik Potsdam (AIP), An der Sternwarte 16, 14482 Potsdam, Germany

Received xxx; accepted yyy

ABSTRACT

Context. An earlier analysis of the Milky Way Star Cluster (MWSC) catalogue revealed an apparent lack of old ($t \gtrsim 1$ Gyr) open clusters in the solar neighbourhood ($d \lesssim 1$ kpc).

Aims. To fill this gap we undertook a search for hitherto unknown star clusters, assuming that the missing old clusters reside at high Galactic latitudes $|b| > 20^\circ$.

Methods. We were looking for stellar density enhancements using a star count algorithm on the 2MASS point source catalogue. To increase the contrast between potential clusters and the field, we applied filters in colour-magnitude space according to typical colour-magnitude diagrams of nearby old open clusters. The subsequent comparison with lists of known objects allowed us to select thus far unknown cluster candidates. For verification they were processed with the standard pipeline used within the MWSC survey for computing cluster membership probabilities and for determining structural, kinematic, and astrophysical parameters.

Results. In total we discovered 782 density enhancements, 522 of which were classified as real objects. Among them 139 are new open clusters with ages $8.3 < \log(t [\text{yr}]) < 9.7$, distances $d < 3$ kpc, and distances from the Galactic plane $0.3 < Z < 1$ kpc. This new sample has increased the total number of known high latitude open clusters by about 150%. Nevertheless, we still observe a lack of older nearby clusters up to 1 kpc from the Sun. This volume is expected to still contain about 60 unknown clusters that probably escaped our detection algorithm, which fails to detect sparse overdensities with large angular size.

Key words. Open clusters and associations: general

1. Introduction

With this paper we continue to present the results of the Milky Way Star Cluster (MWSC) survey undertaken on the basis of the two all-sky catalogues, 2MASS (Skrutskie et al. 2006) and PP-MXL (Röser et al. 2010). The MWSC survey was initiated a few years ago with the aim of building a comprehensive sample of Galactic star clusters with well-determined parameters, which is complete enough to enable an unbiased study of the content and evolution of the star clusters of our Galaxy. The first paper of this series (Kharchenko et al. 2012), called hereafter Paper I, gave an introduction to the survey, explained the underlying motivation, provided a short review of similar studies, described the observational basis of the survey, the data processing pipeline, and presented preliminary results obtained in the second Galactic quadrant. The second paper (Kharchenko et al. 2013, Paper II) summarises the results of the full survey carried out for a compiled input list of 3784 known objects, covering the whole sky. It presents uniform structural, kinematic, and astrophysical data for 3006 open clusters, globular clusters, and compact associations.

The first-look analysis of the MWSC data carried out in Paper II has shown that the MWSC sample is complete up to a distance of $d = 1.8$ kpc from the Sun for clusters of all ages

except the older clusters ($\log(t [\text{yr}]) > 9$). Although this shortage concerns primarily the oldest clusters, the effect can be seen in the general distribution of all Galactic open clusters in Fig. 1, where we show the cluster distribution in the plane $[Z, d_{XY}]$, with Z the vertical distance from the Galactic plane, and d_{XY} the distance from the Sun projected onto the Galactic plane. One can clearly see that at $d_{XY} \lesssim 2$ kpc the number of high-latitude clusters diminishes with decreasing d_{XY} .

The general lack of old open clusters has already been noted in the 1950s (e.g. Oort 1958). Since then, old clusters have been mainly discovered at distances $\gtrsim 1$ kpc, resulting in a striking apparent absence of old clusters in the solar neighbourhood.

There are two main reasons that nearby old open clusters may have escaped previous searches, both based on their proximity.

1. Old open clusters show a larger scale height (van den Bergh & McClure 1980; Froebrich et al. 2010), so in combination with small distances they may be located at higher Galactic latitudes, while systematic searches for open clusters have typically been restricted to areas close to the Galactic plane (e.g. Mercer et al. 2005: $|b| < 1^\circ$; Froebrich et al. 2007: $|b| < 20^\circ$; Glushkova et al. 2010: $|b| < 24^\circ$);

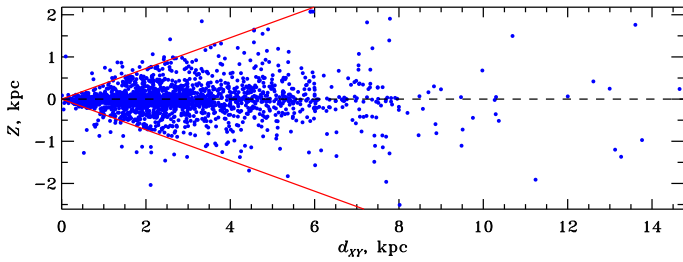


Fig. 1. Distribution of Galactic open clusters from the MWSC survey in the plane (Z, d_{XY}). Solid lines show the limits corresponding to $b = \pm 20^\circ$. The dashed line marks the Galactic plane.

2. With a large angular extent (up to several degrees), they do not stand out prominently as overdensities from the field.

The primary goal of this paper is to get a complete list of clusters within the MWSC survey. To reach this goal we expand previous searches of star clusters in 2MASS performed typically at $|b| \lesssim 20^\circ$ to higher Galactic latitudes. This work can be considered as an extension of the search by Froebrich et al. (2007), which used the same data and a similar approach (without filters), but was restricted to the area $|b| < 20^\circ$.

In Section 2 we describe the data set and our method of identifying clusters. The results are presented in Section 3 and discussed in Section 4.

2. Method

2.1. Data

Cluster candidates were identified as density enhancements in the Two Micron All Sky Survey (2MASS) point-source catalogue (Skrutskie et al. 2006). The 2MASS survey provides the photometric basis of the MWSC survey with a uniformly calibrated photometry of the entire sky, complete down to $K_s \approx 14.3$ mag, depending on the position on the sky. We only considered sources that were detected in all three bands (J, H, K_s) with high quality ($R_{flag} = 1, 2$ or 3). We applied our search algorithm to the entire sky at Galactic latitudes $|b| > 20^\circ$.

2.2. Filtering the sample

Since nearby old clusters may not exhibit a significant overdensity in the plain 2MASS, we had to enhance the contrast between potential clusters and the field. Therefore, we used cuts in colour and magnitude according to typical colour-magnitude diagrams (CMDs) of clusters in different age, distance, and extinction bins. This is an approach comparable, albeit somewhat simpler, to what has been used to detect tidal tails of globular clusters (e.g. Grillmair et al. 1995; Odenkirchen et al. 2003). We set up nine different filters to cover the colour-magnitude space expected for clusters with $0 \lesssim A_{K_s} \lesssim 0.3$ mag and $8.8 \lesssim \log(t \text{ [yr]}) \lesssim 9.4$ at distances around 0.5 and 1 kpc (Fig. 2). This filtering procedure reduces the number of sources in a field to between about 10 and 40 per cent. Figure 3 illustrates the effect of the filtering: While no significant density enhancement can be detected in the unfiltered distribution, a density enhancement above the 4σ level shows up after applying one of the filters. This feature is subsequently confirmed as an open cluster (MWSC 5723).

The filters are not designed to model a specific type of cluster, but to cover the parameter range in the CMD expected for

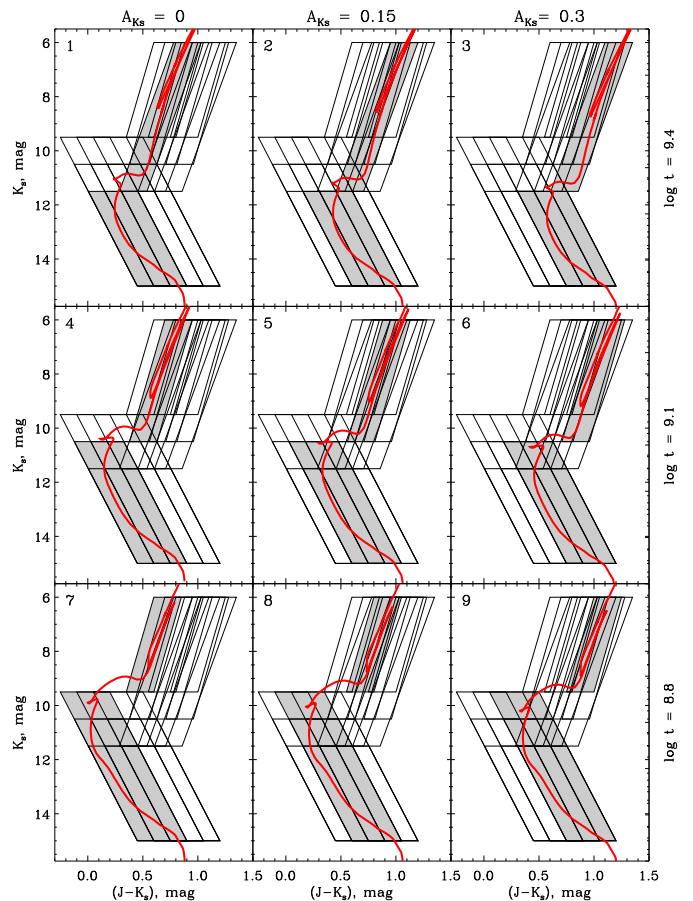


Fig. 2. Nine overlapping filters used to reduce the contamination by field stars. The respective filter is highlighted in grey, the corresponding isochrone for the age and extinction at 1 kpc indicated is shown as a red line. Similar filters were used for a distance of 0.5 kpc. The filter number is given in the upper left corner of each panel.

clusters in the desired age and distance range, to reduce the contamination from unrelated background objects. Since the filters are rather wide, overlap strongly and occupy a wide range, they also cover other parameter combinations, in particular for smaller and larger distances.

2.3. Finding cluster candidates

The filtered sample, together with the unfiltered catalogue, is then used as input for a cluster search algorithm based on star counts (e.g. Carpenter et al. 1995; Lada & Lada 1995; Ivanov et al. 2002; Reylé & Robin 2002). This rather simple approach is nevertheless a very efficient way of creating stellar density maps and identifying density enhancements in a field, comparable to or better than more sophisticated approaches, such as the nearest neighbour density or the separation of minimum spanning trees (Schmeja 2011). We use fields of $5^\circ \times 5^\circ$ in size. Every field is subdivided into a rectilinear grid of overlapping squares that are separated by half the side length of an individual square (the Nyquist spatial sampling interval). The size of the bins is chosen such that they contain 15 stars on average. This results in bins with side lengths between about 3 and 20 arcmin. All areas showing a density $\geq 4\sigma$ above the average density of the field are considered potential clusters, if they contain at least ten sources. Tests showed that bins with a size that on average

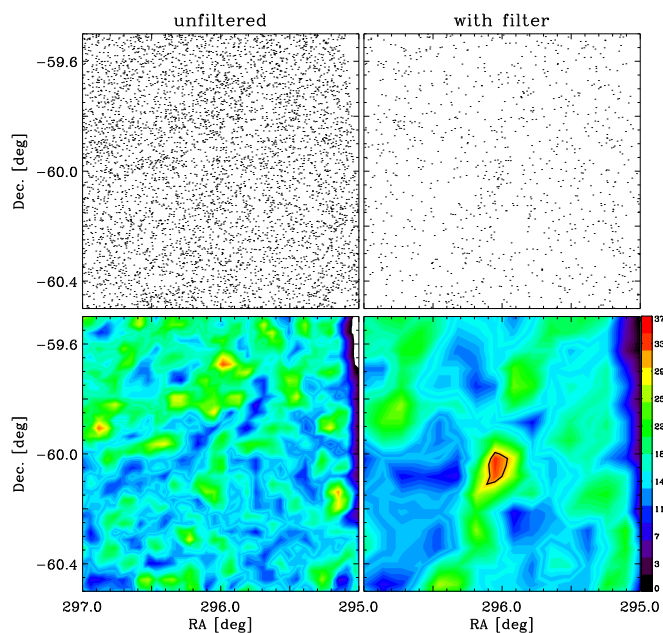


Fig. 3. A $1^\circ \times 1^\circ$ field around the newly found cluster MWSC 5723: 2MASS point sources (upper row) and stellar density maps in number of stars per bin (lower row) for the unfiltered sample (left) and after applying one of the filters (right). The black line on the stellar density map indicates the 4σ contour.

gives 15 stars per bin and an overdensity threshold of 4σ are best suited to detecting clusters without missing a significant number of clusters and picking up too many random density enhancements. Density enhancements that by visual inspection could obviously not be Galactic stellar clusters (such as fragments of M31 or the Magellanic Clouds) were neglected. As a result we prepared a list of candidate clusters that contains the coordinates of the centres of the density enhancements and their sizes.

2.4. Verifying the candidates and determination of the cluster parameters

To be certain that we do not re-discover already known objects, we checked if any candidate was in the MWSC input list, in the SIMBAD data base¹, and because many compact galaxies may appear as point sources in the 2MASS, in the list of galaxy clusters from the Abell et al. (1989) catalogue. The correctness of the preliminary choice of the candidate objects is supported by frequent coincidence of the candidates found with already known objects. The list of unidentified candidates, together with preliminary data on their positions and sizes, was processed with the MWSC pipeline for further checks for the construction of cluster membership and parameter determination.

The pipeline uses kinematic, photometric, and spatial information on stars in the candidate area and is described in more detail in Paper I. The main purpose of the pipeline is to clean a candidate from the fore- and background contamination using kinematic, photometric, and spatial criteria, to produce a list of probable members and to determine the basic cluster parameters in the case of success. The pipeline consists of iterative series of interactive checks of vector point diagram of proper motions, radial density profiles, magnitude-proper motion relation, and various colour-magnitude, two-colour, and Q_{JHK_s} -colour diagrams. As a theoretical basis, we use recent Padova stellar

models of Marigo et al. (2008) and Girardi et al. (2008) with isochrones computed with the CMD2.2 on-line server², whereas the pre-main sequence isochrones were computed by us from the models of Siess et al. (2000) and then transformed to the JHK_s photometric system using transformation tables provided by the Padova team with the *dustyAGB07* database³. The membership probabilities of stars in the diagrams take data accuracy into account and are determined from the star location with respect to the reference sequences (represented either by isochrones or the average cluster proper motion), which themselves depend on the cluster parameters we want to find. This therefore requires an iterative approach, allowing us to successively improve both cluster membership and cluster parameters. The initial approximation was based on a visual inspection of the diagrams. As a rule, the process converges after a few iterations. Including spatial and kinematic criteria greatly helps reduce ambiguities in determining age, distance, and reddening, which may arise if only photometric membership is considered. Details of this effect, called degeneracy, are described in detail in Paper I (Sec. 3.4.3).

The verification of the overdensities as clusters is based on the most probable members only with $P_m > 61\%$ (deviating from the reference by less than one *rms*-error). If their distribution in the vector point diagram of proper motions is more compact than for the rest of the stars, and if they fit the critical points of the isochrone (turn-off, red-giant branch), a candidate is considered to be confirmed, and the most probable members are used for computing the cluster parameters. Otherwise it is rejected as a random clustering of field stars (asterism). The verification by visual inspection of the diagrams is supported by objective statistical arguments. Applying a Fisher test to the identified clusters, we find that the populations of the most probable cluster members ($P_m > 61\%$) and of “field” stars ($P_m < 1\%$) have significantly different dispersions both in the vector point diagram (for 120, or 88% of the clusters) and in the CMD (for all clusters). Figures A.1 and A.2 show the atlas page of an exemplary cluster (MWSC 5224) with its spatial distribution, the radial density profile, the CMDs, and proper motion diagrams.

3. Results

The statistics of results of our cluster search is given in Table 1, which shows the number of candidates, divided into three groups of objects: new real clusters, asterisms, and re-identified known stellar or galaxy clusters. About half of the candidates match known objects: 338 galaxy clusters, 33 globular and 6 Milky Way open clusters, and 8 clusters in the Large Magellanic Cloud. Comparing these statistics to the data present in the catalogues, we can estimate the efficiency of the applied search algorithm. At $|b| > 20^\circ$ there are 49 Galactic globular clusters in the catalogue of Harris (1996, edition 2010). This means that we were able to detect 67% of the known globular clusters. The remain-

² <http://stev.oapd.inaf.it/cgi-bin/cmd>

³ <http://stev.oapd.inaf.it/dustyAGB07/>

Table 1. Classification of star cluster candidates

Object	$b > 20^\circ$	$b < -20^\circ$	All
New clusters	74	65	139
Known objects	206	179	385
Asterisms	134	126	260
Total	414	370	784

¹ <http://simbad.u-strasbg.fr/simbad/>

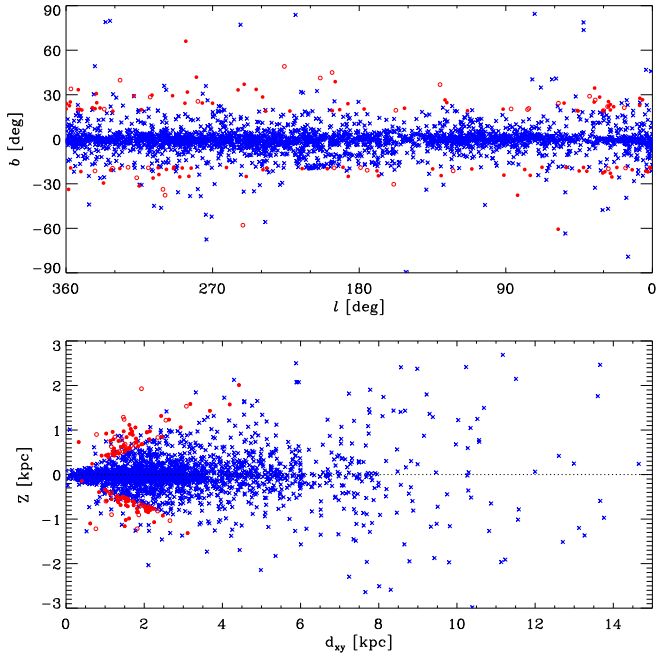


Fig. 4. Distribution on the sky (upper panel) and in the plane (Z, d_{XY}) (lower panel) of known MWSC open clusters (blue crosses) and newly detected clusters (red circles: filled for clusters detected using the filters, open for clusters detected without filters).

ing globular clusters are too faint or too poorly represented in 2MASS to be detected. There were 61 open clusters at $|b| > 20^\circ$ in the MWSC catalogue prior to this work. Excluding associations, moving groups, embedded clusters, and cluster remnants from the sample, there are 18 clusters (called ‘compact’ here), of which we were able to identify six (NGC 188, NGC 2682, NGC 1662, NGC 1980, NGC 2632, and Blanco 1), corresponding to a detection rate of 10% of all open clusters or 33% of the compact clusters. According to the SIMBAD database, there are 26227 clusters of galaxies at $|b| > 20^\circ$. For those our detection rate is of the order of 1% (338). The detection rate of open clusters is therefore ten times higher than the detection rate of clusters of galaxies.

Out of the 139 new clusters, 104 were detected using the CMD filters described in Sec. 2.2, 34 were only found without filters, and one was detected by both applying one of the filters and using the unfiltered field. Since we performed both a filtered and an unfiltered search, we found clusters outside the targeted age and distance limits implied by the filters.

In Fig. 4 we show the distribution of the newly discovered clusters on the sky, together with the previously known open clusters from the MWSC survey. The majority of the confirmed clusters are located within $|b| \lesssim 30^\circ$, though a few open clusters were found up to $|b| \approx 60^\circ$. However, most of the high-latitude candidates turned out to be galaxy clusters.

In Fig. 5 we compare the distributions of the parameters of newly detected clusters and of known high-latitude ($|b| > 20^\circ$) clusters from the MWSC survey. We present the distributions of “structural” parameters, such as the total apparent radius r_2 of a cluster, the apparent radius r_1 of its densest central part, and the tidal radius r_t derived by fitting a King profile to the observed distribution. We also show an empirical estimator of cluster richness n_2 , i. e. the number of the most probable cluster members within r_2 . The lower panel of Fig. 5 shows the distributions of the so-called “photometric” parameters, derived from fitting cluster

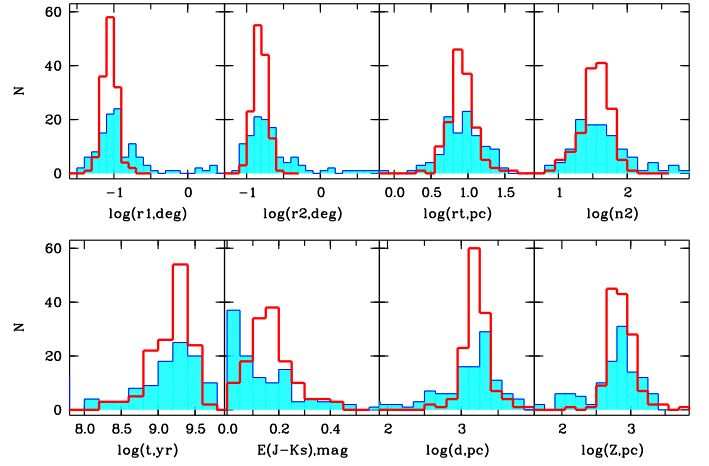


Fig. 5. The distributions of the parameters of new clusters (open red histograms) and of MWSC open clusters at $|b| > 20^\circ$ (blue filled histograms). The upper row compares the distributions of “structural” parameters. The bottom row gives the distributions of “photometric” parameters. See text for an explanation of the definitions.

CMDs: age $\log t$, reddening $E(J - K_s)$, distance $\log d$, and the height Z above the Galactic plane.

The data of the 139 new open clusters have been submitted to the CDS and the GAVO data center as an extension to the MWSC catalogue⁴. The format is the same as that of the MWSC survey in Paper I. An overview with positions, radii, distances and ages of the new clusters is given in Table B.1.

4. Discussion

The initial goal of this search was to find unknown old star clusters at high Galactic latitudes, which might fill the local “hole” around the Sun, as we hoped. The results are illustrated in Figs. 6 and 7 where we compare the distribution of known and new clusters in the XY -plane and show the contribution of new clusters to the surface density of Galactic open clusters.

4.1. The “hole” around the Sun

Figure 6 shows that most of the newly discovered clusters occupy a ring around the Sun with inner and outer borders of $d_{XY} \approx 1$ and 2 kpc (d_{XY} is the cluster distance projected on the Galactic plane), with almost no clusters at $d_{XY} < 1$ kpc. Figure 7 indicates that the new clusters slightly increased (by about 8%) the total surface density. The latter contribute mostly to the surface density of the oldest clusters ($\log t$ [yr] > 9.0), which becomes higher and flatter within the ring. At $d_{XY} < 1$ kpc, the shortage of the oldest clusters is now even more prominent. Assuming the average surface density within the ring to be typical for the whole range of the projected distances d_{XY} , we expect about 50 clusters still to be discovered in the solar vicinity. On the other hand, the new clusters do not significantly affect the surface density distribution of clusters with ages $8.3 < \log t < 9.0$, where a “hole” is only marginally visible at $d_{XY} \lesssim 0.5$ kpc. Possibly about ten clusters are missing in this age and distance range. There is no convincing reason for old clusters to avoid the area around the Sun, therefore it is more likely that they escaped our search because of its limitations as discussed below.

⁴ <http://cdsarc.u-strasbg.fr>; <http://dc.g-vo.org/mwsc-e14a/q/clu/form>

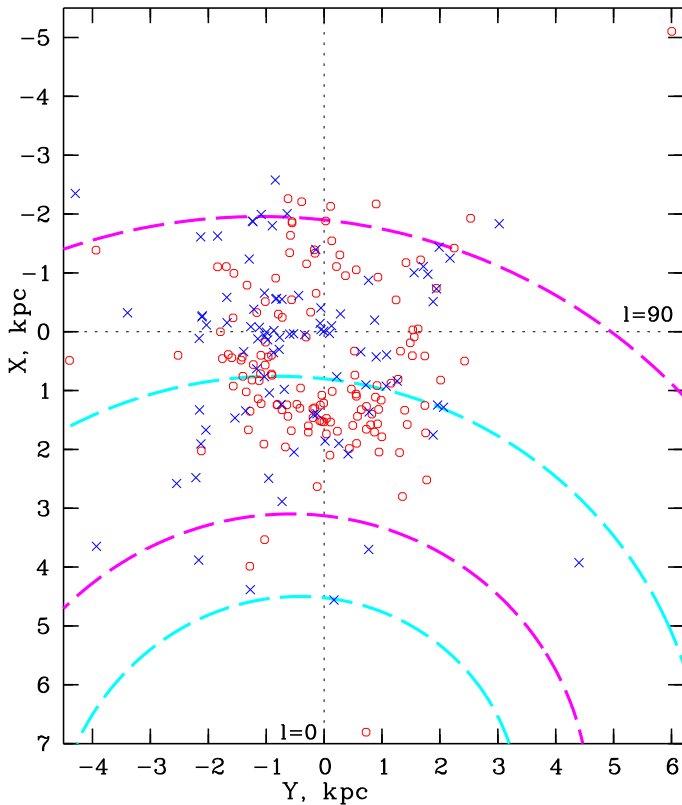


Fig. 6. Distribution of the 139 new clusters (red circles) projected onto the Galactic XY -plane and of known open clusters (blue crosses) selected from the MWSC survey with $\log t = 8.3 \dots 9.7$ and $|b| > 20^\circ$. The dashed spirals indicate the positions of local spiral arms (magenta for Perseus and cyan for Sagittarius) as defined by the COCD clusters (Piskunov et al. 2006).

4.2. Limitations of the search method

Most likely, the missing clusters are just too sparse and too extended to be found as overdensities, even when applying our colour-magnitude filters. For example, it was not possible to detect the cluster Ruprecht 147 ($d = 175$ pc, $\log t = 9.39$, $r_2 = 1:23$; Kharchenko et al. 2005b) with our algorithm. In the area of Ruprecht 147 there are, even when applying our filters, more than 11 000 field stars in 2MASS, compared to about 150 members found for this cluster in the MWSC survey. When only considering the cluster core, there are about 480 field stars compared to 20 cluster members. This is much smaller than the average noise. Even using a very narrow filter specifically tailored to the CMD of Ruprecht 147 instead of our standard filters does not reduce the background to a level where the cluster becomes detectable as an overdensity. Similar to Mercer et al. (2005), who added artificial clusters to their catalogue and tried to recover them, we did additional tests by simulating the Hyades ($d = 45$ pc, $t = 650$ Myr) at different distances between 0.6 and 2 kpc at a latitude of $b \approx 30^\circ$. It turns out that only at distances ≥ 1 kpc is the innermost core ($r \approx 3$ pc) of the cluster detected as a significant overdensity.

We also investigated the effect of our filters on the search. A comparison of the results of both filtered and unfiltered searches (see Fig. 8, showing the distances of new clusters identified with different filters) indicates that the distances do not strongly depend on a specific filter or on its absence. Another experience we gained from the results of this search is that it seems that the presence of cluster members on the giant branch facilitates their

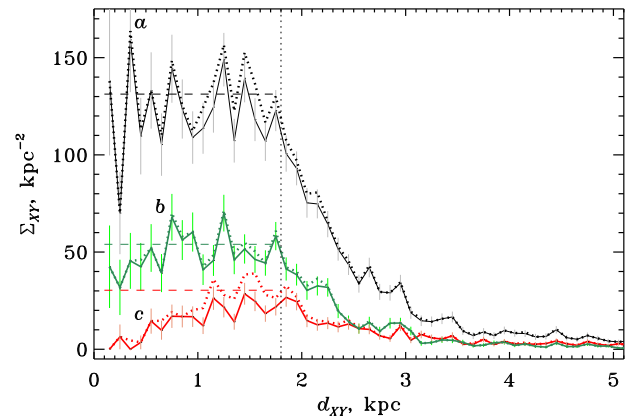


Fig. 7. Contribution of the 139 new clusters to the surface density Σ_{XY} versus the projected distance d_{XY} . The distribution of all clusters is given in black (a), and the distributions of two age groups are indicated with green ($\log t = 8.3 \dots 9.0$, b) and red ($\log t > 9.0$, c). Solid curves correspond to the densities of known open clusters from the MWSC survey, the dotted curves include the new clusters, the dotted vertical line marks the completeness limit found for the total sample, and the dashed horizontal lines correspond to the average surface density for different age groups.

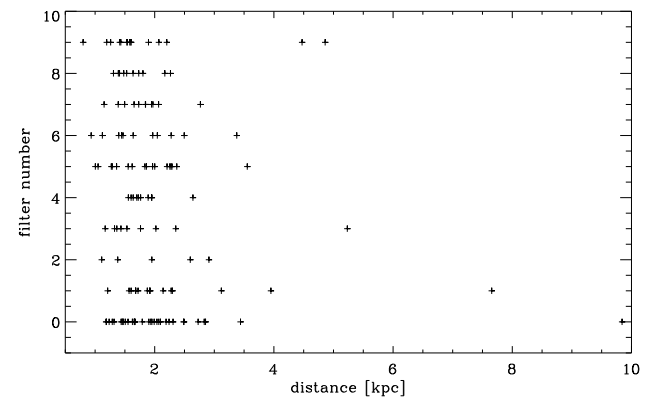


Fig. 8. Filter number (0 = unfiltered search) versus distance of detected clusters. (Usually, a cluster is found in more than one filter, in those cases, the filter is considered where it shows the strongest signal.)

discovery with the filters, so an absence of giants may result in the clusters not being detected.

To estimate the effect of the search method and the underlying catalogue, we compare the distributions with distance of clusters detected in recent optical and NIR surveys (Fig. 9). Both surveys differ by the basic catalogues they use and by the search algorithm. The optical data are represented by the Catalogue of Open Cluster Data (COCD, Kharchenko et al. 2005b,a), based on the catalogue ASCC-2.5, which provides a higher accuracy of kinematic and photometric data and a lower level of background contamination than the combination PPMXL+2MASS does. Unlike the current detection algorithm, the new clusters in this study were searched as density enhancements in the four-dimensional space of proper motions and coordinates in the fields around bright stars ($V < 9$ mag). In the case of MWSC, in addition to the current set of high latitude clusters we consider data on low latitude clusters of Froebrich et al. (2007), which are included in the MWSC input list. While the total distribution of clusters in the NIR-based MWSC extends to higher distances

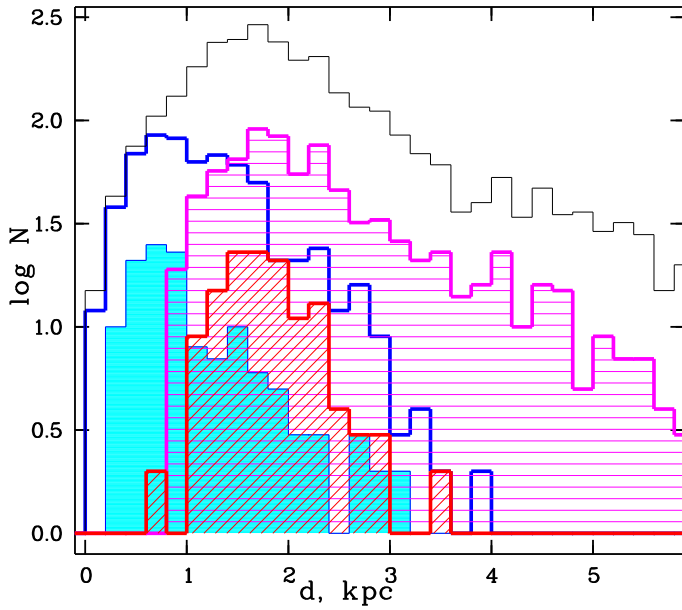


Fig. 9. Comparison of distributions with distance of newly detected clusters for the optical COCD and NIR MWSC surveys. The distributions of new clusters are shown with red (current sample), magenta (candidates of Froebrich et al. 2007), and cyan (Kharchenko et al. 2005a, for COCD). The total distributions are shown with black (MWSC) and blue (COCD).

than those of the optical survey COCD, their subsets of newly identified clusters differ with respect to the lower limit of their distances. While the bulk of new clusters found in the optical reside at distances less than 1 kpc, all the objects detected in the NIR are located outside the 1 kpc limit. This tendency is also seen in other detections of new objects based on the 2MASS catalogue (see e. g. Glushkova et al. 2010). One should note that all these results are based both on the same data source (2MASS) and use a similar approach of searching new clusters as density enhancements in the sky.

Other approaches, such as a search using proper motions (Scholz et al. 2014), may be more successful in finding the missing nearby clusters. In the long run, the *Gaia* mission is expected to fill the gap.

5. Summary

From a first-look analysis of the MWSC in Paper II, we found evidence for a lack of nearby old clusters at high Galactic latitudes and projected distances $d_{XY} \lesssim 1$ kpc. An additional search for star clusters was carried out on the basis of 2MASS and PP-MXL at latitudes $|b| > 20^\circ$. We applied colour-magnitude filters and a star count algorithm to search for these old open clusters. This resulted in the detection of 782 overdensities, regarded as cluster candidates. A comparison with lists of known objects (MWSC input list, SIMBAD data base, and the list of Abell galaxy clusters) has shown that 383 of them are already known objects. The remaining 399 cluster candidates were processed with the standard MWSC pipeline, which confirmed the cluster nature of 139 objects. All of them are open clusters with ages $8.3 < \log t < 9.7$, distances < 3 kpc, and distances from the Galactic plane $0.3 < Z < 1$ kpc. This increased the total number of known high-latitude open clusters by about 150%. Nevertheless, the “hole” with a radius of about 1 kpc around the Sun could not be filled. This dearth of old clusters is expected to be an arte-

fact from the bias against sparse overdensities with large angular size on the sky. We estimate that still about 60 old open clusters are missing in this volume.

Acknowledgements. We wish to thank the referee for a detailed and helpful report. This study was supported by Sonderforschungsbereich SFB 881 “The Milky Way System” (subproject B5) of the German Research Foundation (DFG) and by DFG grant RO 528/10-1. This publication makes use of data products from the Two Micron All Sky Survey, which is a joint project of the University of Massachusetts and the Infrared Processing and Analysis Center/California Institute of Technology, funded by the National Aeronautics and Space Administration and the National Science Foundation. This research has made use of the SIMBAD database, operated at the CDS, Strasbourg, and of the WEBDA database, operated at the Institute for Astronomy of the University of Vienna.

References

- Abell, G. O., Corwin, Jr., H. G., & Olowin, R. P. 1989, *ApJS*, 70, 1
- Carpenter, J. M., Snell, R. L., & Schloerb, F. P. 1995, *ApJ*, 450, 201
- Froebrich, D., Schmeja, S., Samuel, D., & Lucas, P. W. 2010, *MNRAS*, 409, 1281
- Froebrich, D., Scholz, A., & Raftery, C. L. 2007, *MNRAS*, 374, 399
- Girardi, L., Dalcanton, J., Williams, B., et al. 2008, *PASP*, 120, 583
- Glushkova, E. V., Koposov, S. E., Zolotukhin, I. Y., et al. 2010, *Astronomy Letters*, 36, 75
- Grillmair, C. J., Freeman, K. C., Irwin, M., & Quinn, P. J. 1995, *AJ*, 109, 2553
- Harris, W. E. 1996, *AJ*, 112, 1487
- Ivanov, V. D., Borissova, J., Peshev, P., Ivanov, G. R., & Kurtev, R. 2002, *A&A*, 394, L1
- Kharchenko, N. V., Piskunov, A. E., Röser, S., Schilbach, E., & Scholz, R.-D. 2005a, *A&A*, 440, 403
- Kharchenko, N. V., Piskunov, A. E., Röser, S., Schilbach, E., & Scholz, R.-D. 2005b, *A&A*, 438, 1163
- Kharchenko, N. V., Piskunov, A. E., Schilbach, E., Röser, S., & Scholz, R.-D. 2012, *A&A*, 543, A156, (Paper I)
- Kharchenko, N. V., Piskunov, A. E., Schilbach, E., Röser, S., & Scholz, R.-D. 2013, *A&A*, 558, A53, (Paper II)
- Lada, E. A. & Lada, C. J. 1995, *AJ*, 109, 1682
- Marigo, P., Girardi, L., Bressan, A., et al. 2008, *A&A*, 482, 883
- Mercer, E. P., Clemens, D. P., Meade, M. R., et al. 2005, *ApJ*, 635, 560
- Odenkirchen, M., Grebel, E. K., Dehnen, W., et al. 2003, *AJ*, 126, 2385
- Oort, J. H. 1958, *Ricerche Astronomiche*, 5, 507
- Piskunov, A. E., Kharchenko, N. V., Röser, S., Schilbach, E., & Scholz, R.-D. 2006, *A&A*, 445, 545
- Reylé, C. & Robin, A. C. 2002, *A&A*, 384, 403
- Röser, S., Demleitner, M., & Schilbach, E. 2010, *AJ*, 139, 2440
- Schmeja, S. 2011, *Astron. Nachr.*, 332, 172
- Scholz, R.-D., Kharchenko, N. V., Piskunov, A. E., Schilbach, E., & Röser, S. 2014, in preparation
- Siess, L., Dufour, E., & Forestini, M. 2000, *A&A*, 358, 593
- Skrutskie, M. F., Cutri, R. M., Stiening, R., et al. 2006, *AJ*, 131, 1163
- van den Bergh, S. & McClure, R. D. 1980, *A&A*, 88, 360

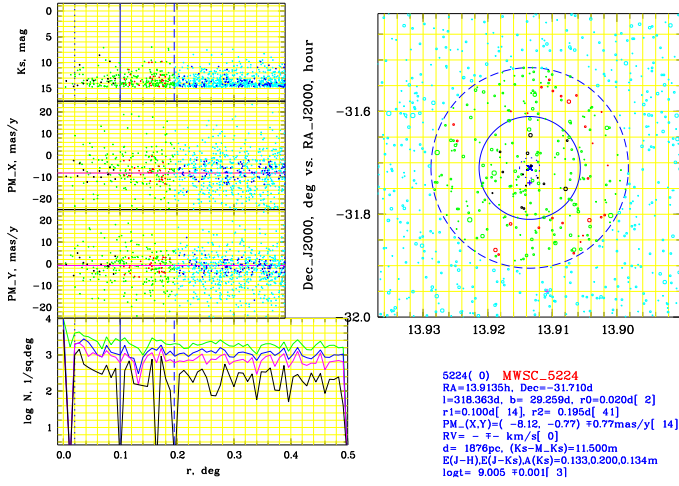


Fig. A.1. Newly found cluster MWSC 5224 in the MWSC Atlas (page 1). Sky map of the cluster region with the most probable members shown in black and red and the radii r_0 , r_1 , and r_2 as dotted, solid, and dashed line, respectively (right panel); K_s magnitude and proper motions versus cluster radius (upper left panels) and radial density profile (lower left panel). See text for a detailed explanation.

Appendix A: Atlas page of MWSC 5244

Figures A.1 and A.2 show the pipeline output for the newly identified cluster MWSC 5224 to illustrate the star member selection procedure and the quality of the determined cluster parameters. The example cluster is selected at random and represents a typical case among the analysed objects.

The main diagram of the first page of the Atlas is a cluster map, while on the second page this role is played by the K_s , $(J-H)$, and K_s , $(J-K_s)$ diagrams. Stars are shown as coloured circles or dots. Symbols and their colours have the same meaning in all plots. Cyan symbols mark stars outside the cluster radius r_2 and green symbols stars within r_2 . The most probable kinematic and photometric members (1σ -members) are indicated in black for members located within r_1 , red for members between r_1 and r_2 , and blue for stars outside r_2 . Cyan bars show the uncertainty for 1σ -members (page 2).

Page 1 of the Atlas (Fig. A.1) contains five diagrams with spatial information, as well as a legend on the derived cluster parameters. The right panel is a map of the cluster surroundings. The left panels show magnitudes K_s , proper motions PM_x , PM_y , and surface density N versus distances r of stars from the cluster centre.

In the sky map, stars are shown by circles. Their size corresponds to the brightness arranged in six K_s magnitude bins. The blue cross indicates the cluster centre determined in this study. If by chance other clusters appear in this area, their centres are marked by magenta plus signs. Large blue circles (shown by dotted, solid, or dashed curves) indicate the cluster radii r_0 , r_1 , and r_2 , respectively. In the left-hand panels, the blue vertical lines (dotted, solid, or dashed) mark r_0 , r_1 , or r_2 . Magenta horizontal lines in the PM vs. r diagrams correspond to the derived average proper motion of the cluster. Radial density profiles in the bottom panel are shown with green for all stars, blue for 3σ -members, magenta for 2σ -members, and black for 1σ -members.

The legend gives cluster name, MWSC number, and COCD number in parentheses; equatorial RA_{J2000} , Dec_{J2000} , and Galactic l , b coordinates of the cluster centre; apparent cluster sizes r_0 , r_1 , r_2 , and number of 1σ -members within the corresponding radius; weighted average components $PM_{X,Y}$ of proper motion

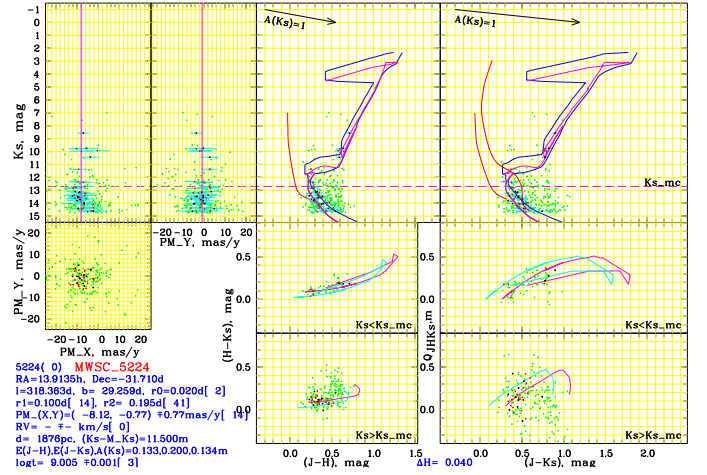


Fig. A.2. Newly found cluster MWSC 5224 in the MWSC Atlas (page 2): Proper motion relations (left panel), CMDs (upper right panels), two-colour diagrams (lower central panels) and Q_{JHK} -colour diagrams (lower right panels). See text for a detailed explanation.

with their *rms* errors and number of stars used to compute the average; the average radial velocity, RV , *rms* error, and the number of stars used to compute the average; distance to the cluster, d , distance modulus, $(K_s - M_K)$; NIR interstellar reddening, $E(J-H)$, $E(J-K_s)$, and interstellar extinction, $A(K_s)$; cluster age, and its *rms* error. The number in brackets gives the number of stars used to compute the average age, or it is -1 if an isochrone fitting was applied. The ΔH shown below the photometric diagrams indicates the empirical correction to the H -magnitude introduced in Paper I.

The parameters are shown as they were derived in the pipeline without taking their real accuracy into account, which was estimated by us from comparison with literature data after the MWSC was completed (for details see Paper II). Typically the cluster proper motions are accurate within 1 mas/yr, and the derived distances and reddenings are accurate within 11% and 7% respectively. An accuracy of the order of 10% is achieved for the ages of older open clusters ($\log(t \text{ [yr]}) > 8.2$).

Page 2 (Fig. A.2) contains three diagrams with kinematic information (left panels), and six diagrams with photometric information (right panels).

The three left panels with kinematic data: the two upper diagrams show $PM_{X,Y}$ vs. K_s relations, i.e. “PM-magnitude equation”. Magenta vertical lines correspond to the average proper motion of the cluster. The magenta dashed line shows the apparent magnitude K_s^{mc} , which corresponds to the bluest colour $(J-K_s)$ of the adopted isochrone. The bottom panel is the vector point diagram of proper motions.

The six right panels with photometric data: the two upper diagrams are CMDs (K_s , $(J-H)$ and K_s , $(J-K_s)$). The magenta curve is the apparent isochrone closest to the determined cluster age. Solid blue lines outline a domain of 100% photometric members. Solid red lines (shown only in K_s , $(J-K_s)$) are the ZAMS (zero-age main sequence) and TAMS (terminal-age main sequence), described in more detail in Paper I. The magenta dashed line shows the apparent magnitude of minimum colour K_s^{mc} . The thick yellow circles mark the stars used for the age determination (see Kharchenko et al. 2005b, for details). The black arrows show the vectors of increasing extinction. The four bottom panels show the two-colour $(H-K_s)/(J-H)$ diagram (left column) and Q_{JHK} -colour diagram (right column). The upper row is for stars brighter than K_s^{mc} , the lower row is

for stars fainter than K_s^{mc} . Magenta curves indicate the apparent isochrone (i.e., apparent colours), whereas cyan curves show the intrinsic isochrone.

The legend is the same as on Page 1.

The atlas pages for all new clusters will be available in electronic form at the CDS and at the GAVO data center⁵.

Appendix B: Table of newly identified clusters

Table B.1 gives an overview of the 139 newly identified clusters. Since the total list of determined parameters is too long (37 columns), we only show the most important parameters here for quick reference (cluster names, equatorial and Galactic coordinates, their total sizes r_2 , distance, and age). The full list of cluster parameters is available in electronic form at the CDS. It is in the same format as the table determined earlier in Paper II for the main body of the MWSC survey.

⁵ <http://dc.g-vo.org/mwsc-e14a/q/clu/form>

Table B.1. The list of newly discovered high-latitude MWSC clusters

Name	RA	Dec	l	b	r_2	distance	age
	[hr] (J2000)	[deg] (J2000)	[deg]	[deg]	[deg]	[pc]	log(t [yr])
MWSC_5004	4.298	86.183	126.223	24.716	0.170	2274	9.215
MWSC_5010	6.305	86.035	127.314	26.485	0.130	3553	9.450
MWSC_5011	6.410	62.630	152.192	20.919	0.155	1272	9.450
MWSC_5012	6.456	57.460	157.507	19.514	0.125	2492	9.085
MWSC_5016	7.154	40.420	176.994	20.373	0.150	2276	8.810
MWSC_5018	7.575	22.825	196.512	19.269	0.145	2070	9.120
MWSC_5019	7.676	32.780	186.948	23.949	0.150	1534	8.970
MWSC_5022	8.273	0.450	222.559	19.021	0.130	1308	9.170
MWSC_5029	8.760	−11.655	237.489	18.928	0.135	1953	9.285
MWSC_5033	8.932	30.155	194.733	38.814	0.205	1530	9.170
MWSC_5038	9.238	23.940	203.901	41.284	0.125	1953	9.300
MWSC_5042	9.351	−7.475	239.297	28.473	0.200	1762	9.500
MWSC_5044	9.419	29.925	196.639	44.974	0.140	2729	9.570
MWSC_5051	9.764	−7.005	243.267	33.615	0.195	1365	9.450
MWSC_5058	10.138	12.318	225.930	49.075	0.230	1191	8.950
MWSC_5060	10.175	−14.045	254.381	33.254	0.190	1445	9.700
MWSC_5062	10.206	−9.181	250.618	37.050	0.120	5232	9.450
MWSC_5071	10.545	−29.585	270.048	24.290	0.150	1965	9.450
MWSC_5076	10.778	78.450	130.371	36.809	0.120	9842	8.850
MWSC_5083	10.933	−32.405	276.330	24.437	0.125	4860	9.200
MWSC_5088	11.146	−32.530	279.044	25.537	0.185	2831	9.225
MWSC_5116	11.651	−36.340	287.001	24.286	0.180	1622	9.515
MWSC_5117	11.672	−17.835	279.955	41.844	0.190	1380	9.360
MWSC_5122	11.732	−28.798	285.506	31.781	0.170	1947	9.500
MWSC_5149	12.280	−32.990	294.589	29.322	0.130	1542	9.500
MWSC_5154	12.416	4.045	286.447	66.068	0.260	799	9.500
MWSC_5186	13.155	−32.970	307.232	29.756	0.205	1947	9.325
MWSC_5191	13.241	−34.190	308.331	28.444	0.161	1318	8.975
MWSC_5215	13.767	−41.843	313.703	19.887	0.175	3118	9.290
MWSC_5224	13.913	−31.710	318.363	29.259	0.195	1876	9.005
MWSC_5231	14.142	−19.465	326.818	39.809	0.160	1935	9.315
MWSC_5273	15.118	−36.361	331.281	18.940	0.165	1599	9.445
MWSC_5279	15.193	−21.428	341.397	30.783	0.200	2066	9.100
MWSC_5289	15.389	−32.490	336.519	20.302	0.185	1672	9.450
MWSC_5292	15.453	−26.487	341.147	24.600	0.150	2276	9.365
MWSC_5293	15.505	−30.440	339.100	21.061	0.165	1414	9.220
MWSC_5295	15.578	−13.380	352.490	33.365	0.170	1764	9.360
MWSC_5299	15.698	−29.000	342.166	20.604	0.130	4473	9.400
MWSC_5300	15.729	−10.300	357.003	33.930	0.195	1506	9.400
MWSC_5301	15.752	−27.510	343.789	21.269	0.150	3950	9.300
MWSC_5309	16.161	−24.440	350.308	19.698	0.185	1724	9.025
MWSC_5311	16.194	−23.215	351.580	20.219	0.155	1410	9.050
MWSC_5312	16.193	−15.960	357.392	25.109	0.170	2910	9.100
MWSC_5316	16.254	−22.370	352.845	20.185	0.210	1390	8.870
MWSC_5318	16.345	−17.235	357.893	22.621	0.150	1169	9.585
MWSC_5319	16.350	−15.143	359.690	23.908	0.165	1326	9.500
MWSC_5321	16.447	−8.927	6.076	26.616	0.140	7655	9.270
MWSC_5323	16.451	−7.170	7.707	27.606	0.170	1925	9.375
MWSC_5326	16.546	−17.143	359.941	20.449	0.180	1637	9.485
MWSC_5329	16.718	−9.840	7.837	22.837	0.175	1111	9.650
MWSC_5333	16.815	16.900	35.462	34.510	0.170	1968	9.350
MWSC_5337	17.124	−3.335	17.276	21.294	0.125	1791	9.390
MWSC_5338	17.130	12.105	32.395	28.423	0.165	2767	9.405
MWSC_5340	17.174	6.425	26.981	25.357	0.170	1361	9.465
MWSC_5343	17.240	17.300	38.555	29.006	0.135	1626	9.355
MWSC_5344	17.258	4.570	25.800	23.398	0.185	1604	9.320
MWSC_5346	17.287	2.212	23.764	21.910	0.180	1952	9.310
MWSC_5348	17.319	13.505	35.107	26.477	0.110	3440	9.500
MWSC_5350	17.367	4.915	26.947	22.112	0.145	1914	9.475

Table B.1. continued.

Name	RA [hr]	Dec [deg]	l [deg]	b [deg]	r_2 [deg]	distance [pc]	age $\log(t \text{ [yr]})$
MWSC_5351	17.387	5.342	27.505	22.041	0.120	1288	9.200
MWSC_5354	17.423	13.465	35.751	25.067	0.210	1004	9.250
MWSC_5356	17.473	2.890	25.813	19.766	0.180	1151	9.205
MWSC_5358	17.619	6.135	29.937	19.304	0.150	1553	9.070
MWSC_5359	17.635	6.618	30.508	19.307	0.130	1721	9.205
MWSC_5365	17.904	28.850	54.222	24.369	0.130	2354	8.985
MWSC_5366	17.986	31.830	57.691	24.307	0.145	1658	9.285
MWSC_5367	18.053	20.102	46.186	19.361	0.155	2044	9.150
MWSC_5368	18.058	19.447	45.574	19.046	0.105	2597	9.255
MWSC_5370	18.721	46.775	75.889	20.739	0.135	1454	9.350
MWSC_5371	18.809	47.235	76.657	20.030	0.140	1902	9.035
MWSC_5373	19.090	56.340	86.739	20.457	0.130	1664	9.100
MWSC_5374	19.305	60.640	91.659	20.270	0.175	1732	9.260
MWSC_5377	21.559	78.256	113.502	19.189	0.160	1434	9.245
MWSC_5901	7.504	27.020	191.995	19.916	0.240	709	9.380
MWSC_5533	0.807	41.600	122.314	-21.271	0.160	2853	8.800
MWSC_5558	1.378	37.965	129.693	-24.499	0.160	2020	9.125
MWSC_5571	1.862	41.500	134.889	-19.971	0.155	1397	9.310
MWSC_5572	1.905	-78.965	299.175	-37.698	0.140	1472	9.300
MWSC_5575	1.995	-83.050	300.483	-33.748	0.150	2191	9.200
MWSC_5602	3.082	23.095	158.811	-30.325	0.155	1184	9.390
MWSC_5604	3.164	-42.880	251.404	-57.905	0.200	1437	9.200
MWSC_5621	3.810	22.270	168.239	-24.630	0.140	1468	9.460
MWSC_5623	4.019	24.115	169.098	-21.307	0.185	1211	9.100
MWSC_5627	4.319	20.335	175.113	-20.867	0.165	1659	9.250
MWSC_5633	4.557	9.400	186.720	-25.025	0.161	1481	9.100
MWSC_5634	4.589	18.540	179.183	-19.105	0.155	1991	9.250
MWSC_5645	5.015	10.445	189.950	-18.875	0.180	2371	9.010
MWSC_5651	5.179	5.890	195.402	-19.263	0.165	2485	9.225
MWSC_5656	5.278	2.210	199.560	-19.873	0.195	1847	8.800
MWSC_5665	6.174	-42.210	249.354	-25.068	0.140	934	8.875
MWSC_5667	6.300	-31.800	239.068	-20.506	0.180	2290	9.015
MWSC_5668	6.326	-29.365	236.763	-19.348	0.180	2141	8.900
MWSC_5670	7.057	-51.205	261.485	-19.043	0.125	1682	8.950
MWSC_5671	7.085	-73.380	284.576	-24.945	0.210	2001	9.400
MWSC_5672	7.255	-78.440	290.189	-25.350	0.135	1288	9.490
MWSC_5674	8.109	-70.325	283.172	-19.443	0.115	1803	9.350
MWSC_5676	8.698	-74.765	288.641	-19.361	0.145	1604	9.150
MWSC_5679	9.550	-78.970	294.025	-19.705	0.155	1122	8.500
MWSC_5680	9.730	-78.205	293.857	-18.786	0.150	1050	9.300
MWSC_5681	10.696	-82.005	298.370	-20.304	0.115	1700	8.980
MWSC_5684	12.895	-86.648	302.966	-23.773	0.155	1432	9.180
MWSC_5685	13.090	-82.043	303.440	-19.182	0.160	1581	9.150
MWSC_5688	15.433	-80.130	309.439	-19.269	0.105	1236	8.990
MWSC_5691	17.436	-70.735	321.885	-18.881	0.100	2241	8.350
MWSC_5692	17.789	-86.610	306.560	-26.142	0.135	1555	8.930
MWSC_5694	17.956	-66.800	326.935	-19.698	0.110	1570	9.000
MWSC_5696	18.188	-62.815	331.444	-19.549	0.120	2308	8.550
MWSC_5697	18.410	-62.195	332.632	-20.778	0.125	1496	9.250
MWSC_5698	18.697	-77.723	316.596	-25.947	0.150	2069	8.890
MWSC_5701	18.826	-53.860	342.212	-21.337	0.130	1467	8.750
MWSC_5704	19.073	-39.930	357.158	-19.329	0.110	1604	9.370
MWSC_5705	19.115	-46.272	350.885	-21.768	0.120	1861	8.950
MWSC_5706	19.160	-35.860	1.583	-18.918	0.140	1558	8.990
MWSC_5708	19.199	-36.315	1.303	-19.518	0.100	1844	8.575
MWSC_5712	19.422	-34.475	4.119	-21.474	0.140	1654	8.745
MWSC_5713	19.426	-35.820	2.762	-21.945	0.095	2265	9.115
MWSC_5715	19.559	-26.895	12.402	-20.564	0.150	2170	8.360
MWSC_5717	19.578	-22.888	16.469	-19.336	0.105	2097	8.775
MWSC_5720	19.695	-18.105	21.810	-19.004	0.110	1639	9.360

Table B.1. continued.

Name	RA [hr]	Dec [deg]	l [deg]	b [deg]	r_2 [deg]	distance [pc]	age $\log(t \text{ [yr]})$
MWSC_5723	19.701	−60.015	337.003	−29.497	0.150	1195	9.130
MWSC_5726	19.890	−13.960	27.037	−19.919	0.135	2038	8.900
MWSC_5731	20.047	−16.220	25.792	−22.905	0.155	3377	9.265
MWSC_5732	20.069	−12.928	29.186	−21.863	0.160	2203	8.650
MWSC_5735	20.156	−12.185	30.489	−22.722	0.125	1970	9.250
MWSC_5737	20.184	−17.940	24.876	−25.370	0.135	2495	8.925
MWSC_5740	20.262	−0.630	42.304	−18.954	0.135	2255	8.825
MWSC_5744	20.339	−42.245	358.445	−33.757	0.115	1836	9.220
MWSC_5745	20.351	−3.530	40.258	−21.511	0.140	1639	9.080
MWSC_5748	20.483	0.400	44.977	−21.355	0.150	1388	8.725
MWSC_5749	20.536	−78.615	315.018	−31.446	0.150	1890	9.345
MWSC_5751	20.596	7.985	52.837	−18.912	0.140	1532	9.250
MWSC_5764	21.160	19.486	67.765	−18.873	0.120	2297	9.200
MWSC_5779	21.729	25.820	78.371	−20.392	0.135	2642	9.130
MWSC_5782	21.767	20.830	75.002	−24.327	0.150	1732	9.290
MWSC_5800	22.606	30.240	91.168	−24.177	0.160	1679	8.325
MWSC_5804	22.732	15.040	82.777	−37.695	0.200	1896	9.465
MWSC_5811	23.051	−12.315	57.842	−60.611	0.240	1261	9.425
MWSC_5828	23.845	41.428	110.860	−20.019	0.180	2207	9.200
MWSC_5963	5.732	−10.655	215.029	−19.770	0.250	430	8.820